

Residual stress prediction in hard machining: A comparative study of ANN, ANFIS, SVM and GPR models

Article Info:

Article history: Received 2024-07-08 / Accepted 2024-12-27 / Available online 2024-12-27

doi: 10.18540/jcecv110iss8pp21107



Zaki Adelfetah Abed

ORCID: <https://orcid.org/0009-0004-4732-1335>

Research Laboratory of Industrial Technologies, Faculty of Applied Sciences, University of Tiaret,
B. P. 78 Zaâroua 14000 Tiaret, Algeria
E-mail: abedzakiabdefetah@gmail.com

Kamel Haddouche

ORCID: <https://orcid.org/0000-0002-7084-0246>

Research Laboratory of Industrial Technologies, Faculty of Applied Sciences, University of Tiaret,
B. P. 78 Zaâroua 14000 Tiaret, Algeria
E-mail: haddouchekam@gmail.com

Sahraoui Aissat

ORCID: <https://orcid.org/0000-0002-6141-9396>

Research Laboratory of Industrial Technologies, Faculty of Applied Sciences, University of Tiaret,
B. P. 78 Zaâroua 14000 Tiaret, Algeria
E-mail: sh_aissat@yahoo.fr

Souâd Makhfi

ORCID: <https://orcid.org/0009-0001-3883-4567>

Research Laboratory of Industrial Technologies, Faculty of Applied Sciences, University of Tiaret,
B. P. 78 Zaâroua 14000 Tiaret, Algeria
E-mail: msouad71@gmail.com

Malek Habak

ORCID: <https://orcid.org/0000-0003-1498-4680>

Laboratory of Innovate Technologies, Picardie Jules Verne University, Avenue des Facultés, Le
Bailly 80025 Amiens Cedex 1, France
E-mail: malek.habak@u-picardie.fr

Abstract

In the present investigation, techniques based on learning are applied to predict longitudinal and circumferential residual stresses during the hard turning of AISI 52100 steel by a CBN cutting tool. Residual stresses are one of the most commonly variables which evaluate the machined surface integrity. Predicting this last is a major objective related to the quality and life of manufactured products. In this context, we use four models to estimate residual stresses: Artificial Neural Network (ANN), Adaptive Neuro-Fuzzy Inference System (ANFIS), Support Vector Machine (SVM), and Gaussian Process Regression (GPR). The analysis is based on experimental data structured in 34 combinations using work material J-C rheological properties (A, B and n) and cutting parameters (V_c , f and a_p). These rheological properties are related to the hardness and microstructure, which depend respectively on the heat treatment and carbide inclusion. For the developed models, ANFIS gives globally the best performances, achieving high value of R^2 and minimal MSE; it shows the most promise of prediction. This underscores the effectiveness of learning techniques in estimating residual stresses.

Keywords: Residual stresses. Hard machining. AISI 52100 steel. CBN cutting tool. Learning techniques. ANN. ANFIS. SVM. GPR.

1. Introduction

Hard turning attempts to replace grinding and increase the integrity of the machined surface. It allows hard materials to be machined directly, removing the need for lubricant and favoring dry machining (Sivaraman *et al.*, 2017). Among the many unresolved problems with hard turning is the creation of undesirable residual stress patterns and white layers on the machined surface. Residual stresses, roughness and microstructure are the most commonly variables which evaluate surface integrity. Predicting surface integrity is a major objective related to the quality and life of machined products. Understanding the intricate relationships between microstructure, mechanical state, modes of failure, and structural integrity depends critically on the precise calculation of residual stresses (Tabatabaeian *et al.*, 2022).

Both tensile and compressive residual stresses can be produced by mechanical load, while the thermal effect on the surface layer can only yield tensile residual stress (Sutanto *et al.*, 2018). The relation between the mechanical as well as thermal phenomena in production of residual stress during machining operations is reported in (Outeiro *et al.*, 2018). The mechanical performance may be reduced by the residual stresses, and the parts may even fail before their life. As is often known, residual stresses can result in a variety of engineering issues, including distortions, cracks, etc. when their magnitudes exceed ultimate strength and fatigue. One of precision machining's challenges is the possibility for parts to deform as a result of residual stresses from machining operations or while under working conditions (Soori *et al.*, 2022). In addition, residual stresses occur in the surface and subsurface layers of machined components. Therefore, it is necessary to examine the mechanical state of the machined surface as well as the subsurface. A workpiece's final state of residual stress is determined by its material, the cutting tool configuration (including tool geometry and coating), cooling, wear, and process variables (such as cutting speed, feed rate, and depth-of-cut (Elsheikh *et al.*, 2022).

Recently, the hard steel AISI 52100 which is the subject of our study continues to give rise to various investigations, some of which we will mention below. Paschoalinoto *et al.* (2021) have studied the effect of process parameters and cutting tool shape on residual stress of AISI 52100 hard steel turned by high-speed machining with three different conventional inserts. Kokkiralala *et al.* (2022) investigated the effect of cutting conditions on the generated surface integrity of hard-turned martensitic AISI 52100 bearing steel. The studied cutting conditions are cutting speed, chamfer angle, feed rate and depth-of-cut. The study of (Kara *et al.*, 2023) covers tensile, fatigue, and material characterization tests on AISI 52100 material. In their study, they investigate how the material's mechanical characteristics (macro-hardness, micro-hardness, yield, and tensile strength), microstructure, change in residual austenite volume ratio, and residual stress values are affected by deep cryogenic treatment (DCT) applied at varying holding hours. Ajay *et al.* (2020) found that hybrid nanofluid MQCL enhances the overall performance of the machined surface as compared to other near-dry techniques. In addition, Hüseyin Alp *et al.* (2024) investigated the performance of conventional and wiper CBN inserts under various cooling conditions during hard turning of AISI 52100 steel. Huang *et al.* (2023) studied the effects of multi-pass turning on surface properties of AISI 52100 bearing steel. For example, double pass turning significantly reduces the residual stress of machined surface. Pawar *et al.* (2017) investigated numerical modeling under Abaqus software to determine the effect cutting speed and depth-of-cut on induced residual during the turning of AISI 52100.

To increase production efficiency, improving product quality and reducing costs, new breakthroughs need the employment of enhanced predictive models in process-planning systems for the machining processes. This has led to the development of various approaches: analytical, numerical, experimental, and AI-based techniques. In this study, we will develop four predictive models using some AI techniques to estimate both axial (σ_{xx}) and circumferential (σ_{yy}) residual stresses during the hard turning of AISI 52100 steel by a CBN cutting tool. The developed models use Artificial Neural Network

(ANN), Adaptive Neuro-Fuzzy Inference System (ANFIS), Support Vector Machine (SVM), and Gaussian Process Regression (GPR). The analysis is based on experimental data structured in 34 combinations of material hardness (HRC), rheological properties (A, B and n) and cutting parameters (V_c , f and a_p). To enhance the efficacy of the developed models, we used some performance indicators such as the R-squared statistic- R^2 , Mean Square Error-MSE and Mean Absolute Percentage Error-MAPE.

2. Modeling

2.1 ANN Approach

ANN approach is widely used for modeling a nonlinear relationship due to their ability to learn patterns from observed data. A typical ANN utilizes a multilayer architecture organized in: an input layer, one or more hidden layers, and an output layer. Equation 1 gives the mathematical expression of the neuron output s_j (Hagan *et al.*, 2014) as follows:

$$s_j = g \left(\sum_{i=1}^m w_{ij} \cdot x_i - b_j \right) \quad (1)$$

If the activation level of a neuron exceeds the bias b_j , the output of the transfer function g obtained from the sum of weighted inputs receipts a value equal to +1; otherwise, it takes zero. The bias can be likened to a weight assigned to a constant input of -1. The weights w_{ij} of inputs x_i and b_j are tuned coefficients. To concept the network, the dataset is separated into two distinct subsets: one for training and another for testing. A training algorithm is used to tune w_{ij} and b_j in order to found the desired relationship between input and output. Users can select the transfer function, specify the hidden layers and neurons number, and determine the training algorithm to achieve optimal performances.

2.2 ANFIS model

Jang *et al.* (1993) developed the ANFIS model; it is a kind of ANN based on the inference system of Takagi-Sugeno. ANFIS uses principally five layers to establish the relationship between the inputs and outputs through hybrid learning. The inputs are processed by the membership functions in Layer 1; in this context, different functions can be used: triangular, Gaussian, etc. The nodes of Layer 1 are adaptive. The fuzzification is done in the Layer 2; every node in this layer is a fixed node labeled (Π), whose output results of the product of the incoming signals. In Layer 3, rules are applied to the outputs coming from Layer 2. In this layer, the fixed nodes represent the normalized firing strengths of the rules, ensuring that the contributions of each rule are appropriately weighted. The defuzzification is done in Layer 4 by adaptive nodes. Finally, the single node in Layer 5 is a fixed node labeled (Σ), which computes the overall output as the summation of all incoming signals.

In the case of the ANFIS with two inputs x_1 and x_2 , the following equations show the outputs for the five layers:

$$L_{1,i} = \mu A_i(x_1), \quad \text{for } i = 1, 2 \dots j \quad (2)$$

$$L_{1,i} = \mu B_i(x_2), \quad \text{for } i = 1, 2 \dots j \quad (3)$$

$$L_{2,i} = W_i = \mu A_i(x_1) \cdot \mu B_i(x_2), \quad \text{for } i = 1, 2 \dots j^2 \quad (4)$$

$$L_{3,i} = \bar{W}_i = \frac{W_i}{\sum_{i=1}^{j^2} W_i} \quad (5)$$

$$L_{4,i} = \bar{W}_i f_i = \bar{W}_i (p_i x_1 + q_i x_2 + r_i) \quad (6)$$

$$L_{5,i} = \sum_{i=1}^{j^2} \bar{W}_i f_i = \frac{\sum_{i=1}^{j^2} W_i f_i}{\sum_{i=1}^{j^2} W_i} \quad (7)$$

Where μ_{A_i} and μ_{B_i} are the membership functions and (p_i, q_i, r_i) are the linear parameters of ANFIS.

2.3 SVM

Support Vector Machine (SVM) is a supervised learning approach aimed at finding an optimal hyperplane that separates data into two groups. Then, it maximizes the margin by creating two parallel boundary planes, with support vectors being the closest observations to these boundaries (Cortes *et al.*, 1995; Cristianini *et al.*, 2000; Deng *et al.*, 2017; Gholami *et al.*, 2017; Gunn *et al.*, 1998; Hsu *et al.*, 2010; Salcedo-Sanz *et al.*, 2014; Vapnik *et al.*, 1998).

Using kernel functions, SVM maps input-data into a high-dimensional space where a linear model is then constructed. Like the ANN, the data must be organized into training and test datasets and the estimations will be produced after the training. Lastly, the model's parameters will be calculated, counting the support vector, the coefficients and bias in order to determine the regression function agreeing to Equation 8:

$$y = \sum_{i=1}^n \alpha_i K(X_i, x) + b \quad (8)$$

Where α_i are the computed parameters, K is the kernel function, X_i is the support-vector, and b is the bias.

2.4 GPR model

Gaussian processes are a versatile nonparametric supervised learning technique widely used for probabilistic classification and regression problems. They offer several advantages, such as interpolating data when using standard kernels, allowing for accurate predictions. For a training dataset with input x_i and observed quantities y_i , Equation 9 (Isabona *et al.*, 2023; Schulz *et al.*, 2018) gives the model:

$$y_i = f(x_i) + \zeta_i \quad (9)$$

Where $\zeta_i = N(0, \sigma_i^2)$ is the mean noise with σ_i^2 variance. For a Gaussian distribution, the observed value is expressed by using Equation 10:

$$(x_i) \approx GP(m(x_i), \bar{K}(X, X')) \quad (10)$$

With $\bar{K}(X, X')$ is the covariance matrix and $m(x_i) = E[f(x_i)]$ is an expectation function of the input.

3. Experimental data

Habak (2006) collected the experimental data during the dry hard turning of AISI 52100 steel with a CBN cutting tool BNX10 (2-NU VBGW160408 of Sumitomo) (Habak, 2006). The chemical composition of parts was verified using a spark emission spectrometer. Table 1 shows the chemical composition of the workpiece.

Table 1 – Chemical composition of work material (Habak, 2006).

Element (%)	C	Cr	Cu	S	Si	Mo	Mn	P
Measured value	1.05	1.481	0.033	0.018	0.239	0.01	0.365	0.009

To obtain tubes with the presence of undissolved carbides, the samples were austenitized at 850 °C in a furnace for 30 minutes and then soaked with water at 30 °C. Several tempering temperatures were chosen to obtain tubes of different hardness values. In order to dissolve all the carbides, the tubes were austenitized at 1000 °C (the dissolution temperature of all carbides), followed by isothermal processing in a salt bath furnace at 225 °C for 7 hours, to obtain a hardness of 55 HRC. Temperatures were maintained at different temperatures in order to have different hardnesses.

Figure 1 shows the microstructures of AISI 52100 steel (55 HRC) with and without carbides.

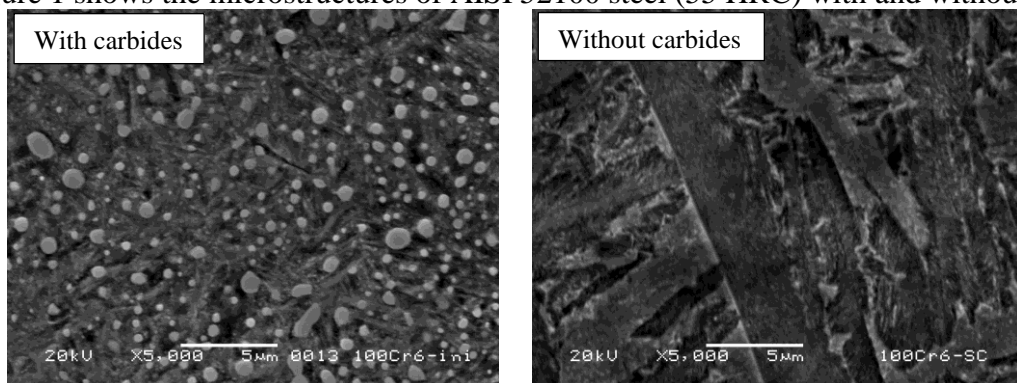


Figure 1 – Microstructures of work material (Habak, 2006).

The axial (σ_{xx}) and circumferential (σ_{yy}) residual stresses are measured by X-ray diffraction while considering different hardness of the work material and carbides inclusion. The device used for residual stress analysis is a portable Proto diffractometer. The X-ray generating tube used for the machined material consists of a Cr anode. The collimator used has a diameter of 1 mm and the voltage used is 20 kV for an intensity of 4 mA. Figure 2 shows the residual stress analysis directions.

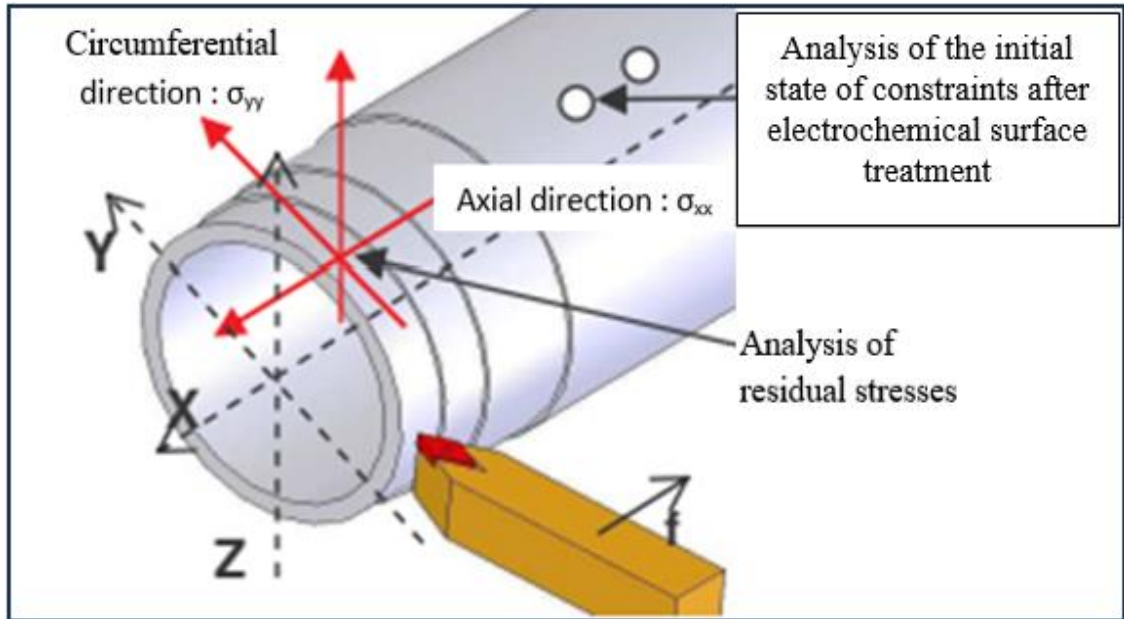


Figure 2 - Residual stress analysis directions (Habak, 2006).

The following equations show the dependence on hardness and carbides inclusion (Habak, 2006) of the rheological coefficients (A, B and n) of work material according to Johnson-Cook law:
Work material with carbides:

$$A = 1.778 \times HRC^2 - 120.67 \times HRC + 3383.9 \quad (11)$$

$$B = 5.3889 \times HRC^2 - 409.83 \times HRC + 7999.4 \quad (12)$$

$$n = -0.0014 \times HRC^2 + 0.1637 \times HRC - 4.2522 \quad (13)$$

Work material without carbides:

$$A = 11.5 \times HRC^2 - 1091.5 \times HRC + 27345 \quad (14)$$

$$B = 16.5 \times HRC^2 - 1556.5 \times HRC + 37195 \quad (15)$$

$$n = 0.0016 \times HRC^2 - 0.1393 \times HRC + 3.3178 \quad (16)$$

The data are structured in 34 combinations considering the rheological coefficients (A, B, n) and cutting parameters (cutting speed V_c , feed f , depth-of-cut a_p). Dataset of 24 samples are used for the training phase, while the remaining 10 samples are reserved for testing (Tables 2 and 3).

Table 2 - Training dataset (Makhfi, 2018).

Carbides inclusion	Test n°	Rheological coefficients			Cutting parameters			Experimental residual stresses	
		A (MPa)	B (MPa)	n	V _c (m/min)	f (mm/tr)	a _p (mm)	σ _{xx} (MPa)	σ _{yy} (MPa)
With carbides	1	1492	357	0.21	150	0.1	0.2	106	94
	2	2179	1891	0.52	50	0.1	0.2	54	-98
	3	2179	1891	0.52	150	0.05	0.2	-205	-205
	4	2179	1891	0.52	150	0.1	0.2	-24	-116
	5	2179	1891	0.52	200	0.1	0.2	-114	-20
	6	2179	1891	0.52	300	0.1	0.2	-29	207
Without carbides	7	1515	565	0.29	100	0.1	0.25	-78	-60
	8	1515	565	0.29	100	0.1	0.2	21	103
	9	1515	565	0.29	150	0.05	0.2	20	43
	10	1515	565	0.29	150	0.1	0.3	119	226
	11	1515	565	0.29	150	0.12	0.1	8	-172
	12	1515	565	0.29	150	0.15	0.2	218	224
	13	1515	565	0.29	150	0.2	0.2	200	-52
	14	1515	565	0.29	200	0.1	0.2	10	2
	15	1634	797	0.39	100	0.1	0.2	-138	-329
	16	1938	1258	0.46	100	0.1	0.2	-154	-186
	17	1938	1258	0.46	150	0.05	0.2	-232	-131
	18	1938	1258	0.46	150	0.1	0.4	-286	103
	19	1938	1258	0.46	150	0.15	0.2	-330	-523
	20	1938	1258	0.46	150	0.2	0.2	-218	-309
	21	1938	1258	0.46	200	0.1	0.2	-173	109
	22	2144	1258	0.51	100	0.1	0.2	-240	-331
	23	2144	1566	0.51	250	0.1	0.2	-324	-346
	24	2144	1566	0.51	300	0.1	0.2	-116	473

Table 3 - Testing dataset (Makhfi, 2018).

Carbides inclusion	Test n°	Rheological coefficients			Cutting parameters			Experimental residual stresses	
		A (MPa)	B (MPa)	n	V _c (m/min)	f (mm/tr)	a _p (mm)	σ _{xx} (MPa)	σ _{yy} (MPa)
With carbides	25	2179	1891	0.52	150	0.15	0.2	-17	-99
	26	2179	1891	0.52	200	0.1	0.1	-68	-244
	27	2179	1891	0.52	250	0.1	0.2	-127	48
Without carbides	28	1515	565	0.29	150	0.08	0.2	96	131
	29	1515	565	0.29	150	0.1	0.2	0	23
	30	1634	797	0.39	150	0.1	0.2	-83	113
	31	1938	1258	0.46	150	0.1	0.2	-188	-28
	32	1938	1258	0.46	150	0.1	0.3	-379	108
	33	2144	1566	0.51	150	0.1	0.2	-479	-523
	34	2144	1566	0.51	200	0.1	0.2	-280	-297

According to (Habak, 2006), from all the analyses, it appeared that cutting speeds ranging from 150 m/min to 250 m/min for the AISI52100 with carbides and from 100 to 250 m/min for the carbide free and low feed favor the generation of compressive residual stresses on the extreme surface. In addition to these parameters, the work material without carbide and high hardness help in the formation of compressive stresses and the generated surface is more hardened.

4. Simulation results

All predictive simulations for axial and circumferential residual stresses were conducted by using the Matlab 2023b software under an HP workstation Z840.

4.1 ANN Approach

In the present study, we use a developed script and we consider a feedforward-net with a single hidden layer. We chose a linear transfer function for the output and a hyperbolic tangent sigmoid function for the hidden layer for obtaining best performances (Makhfi *et al.*, 2018; Mimoun *et al.*, 2022, Djellouli *et al.*, 2023). The used training function is the Bayesian Regularization backpropagation; it takes longer but may be better for challenging problems. After launching the training phase for different numbers of hidden neurons as reported in Table 4, the optimal configuration is given for 6-10-2 structure consisting of six inputs (A, B, n, V_c , f and a_p), ten hidden neurons and two outputs (σ_{xx} and σ_{yy}).

Table 4 – Choice of the number of hidden neurons.

Structure	R training	MSEN
6-3-2	0.87986	0.05987160
6-4-2	0.90244	0.04934075
6-5-2	0.90275	0.04922082
6-6-2	0.91102	0.04533624
6-7-2	0.91190	0.04488204
6-8-2	0.91186	0.04492846
6-9-2	0.91195	0.04487994
6-10-2	0.91293	0.04436313
6-11-2	0.90701	0.04705184

The following figure shows the training performance for the 6-10-2 ANN architecture.

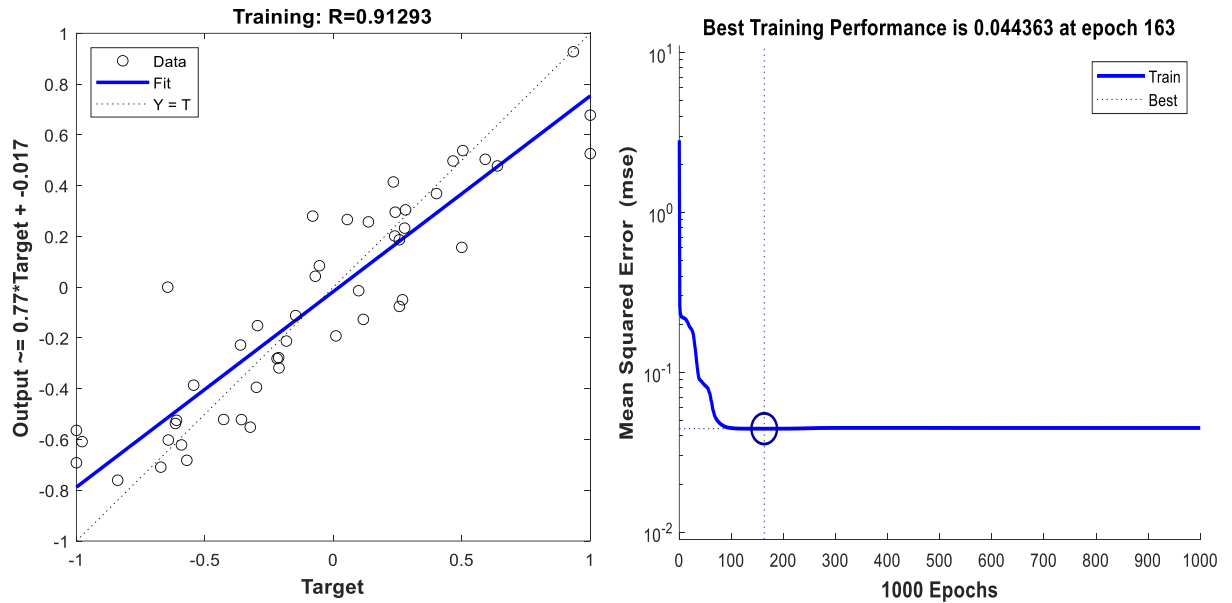


Figure 3 – ANN training for the 6-10-2 structure.

Figure 3 indicates that the model reaches best training performance at epoch 163 with a normalized MSE equal to 0.044363 and correlation coefficient $R = 0.91293$. However, deviations from the ideal line ($Y = T$) may be attributed to the complexity of the phenomena being modeled.

4.2 ANFIS model

The ANFIS structure is created with six inputs for each residual stress. We used the Neuro-Fuzzy Designer under Matlab by considering Sugeno’s Fuzzy Inference System (FIS), which is generally recognized as well suited for modeling nonlinear systems. We tested various FIS to identify the optimal configuration for predicting residual stresses. To achieve best performances, the configuration 4-4-4-4-4-2 is done for σ_{xx} , and the structure 4-4-5-5-5-2 is chosen for σ_{yy} . In addition, a triangular membership function is applied to inputs and constant membership function is done for the output. The simulation is stopped at 20 epochs by using a grid-partition and hybrid optimization method that combines least squares and backpropagation. Figures 4 and 5 show respectively the training phases for the residual stresses σ_{xx} and σ_{yy} . The training data and the FIS output are much correlated.

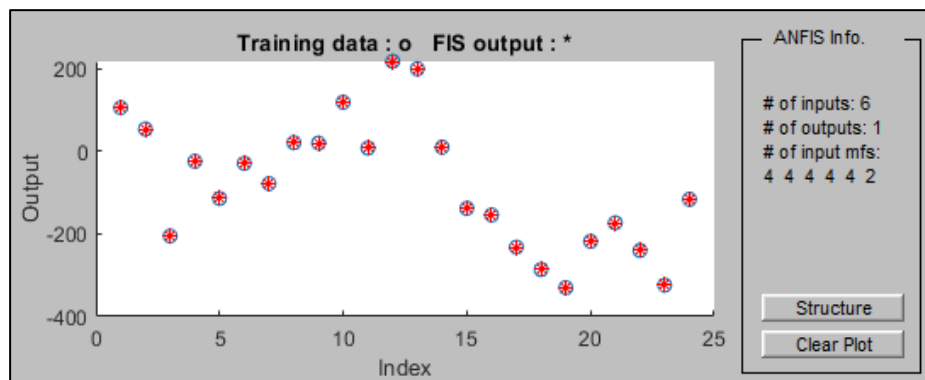


Figure 4 - ANFIS model for σ_{xx} (training phase).

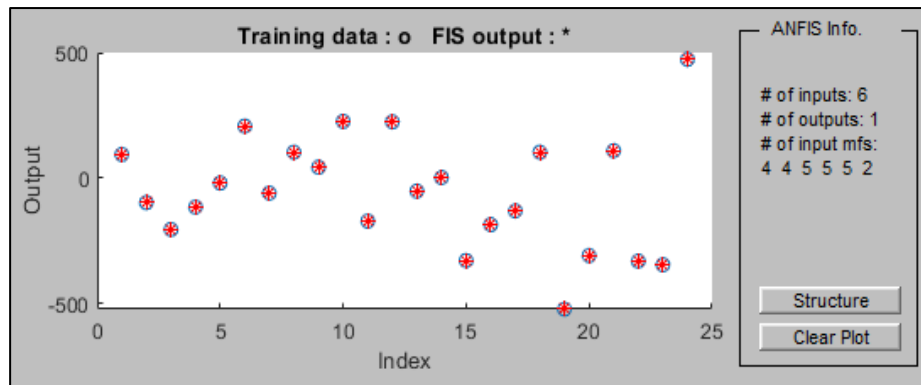


Figure 5 - ANFIS model for σ_{yy} (training phase).

Figures 4 and 5 indicate that the ANFIS models reach a best training performance.

4.4 SVM model

In the training phase by using Regression Learner under Matlab, several kernel functions were tested including coarse Gaussian, medium Gaussian, fine Gaussian, cubic, quadratic and linear SVM. However, we selected the cubic kernel due to its superior performance in both training and testing phases compared to the other kernel functions. For simulation, we consider resubstitution validation and default model hyper-parameters: Box constraint “auto mode”, Epsilon “auto mode”, Kernel scale “auto mode”, Standardize “yes”. Figures 6 and 7 show the prediction for the residual stresses σ_{xx} and σ_{yy} for training phase.

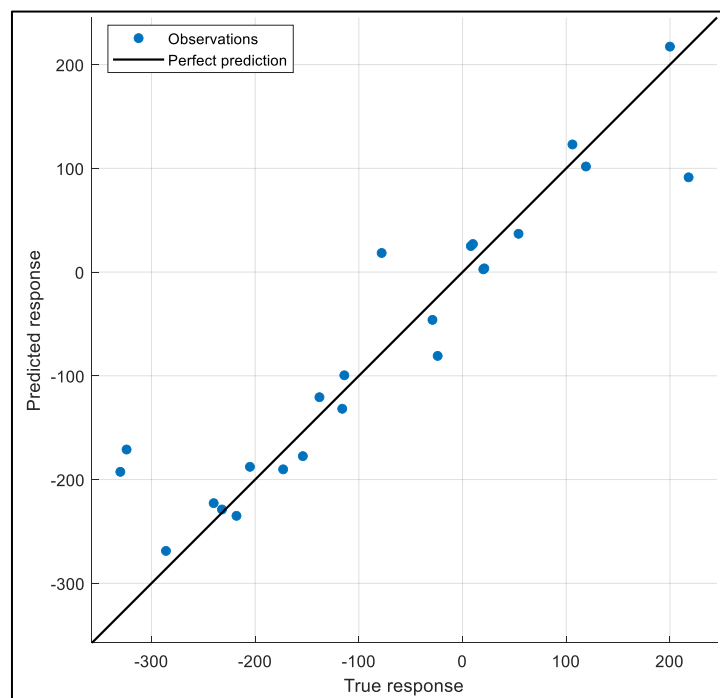


Figure 6 - SVM model for σ_{xx} (training phase by cubic kernel function).

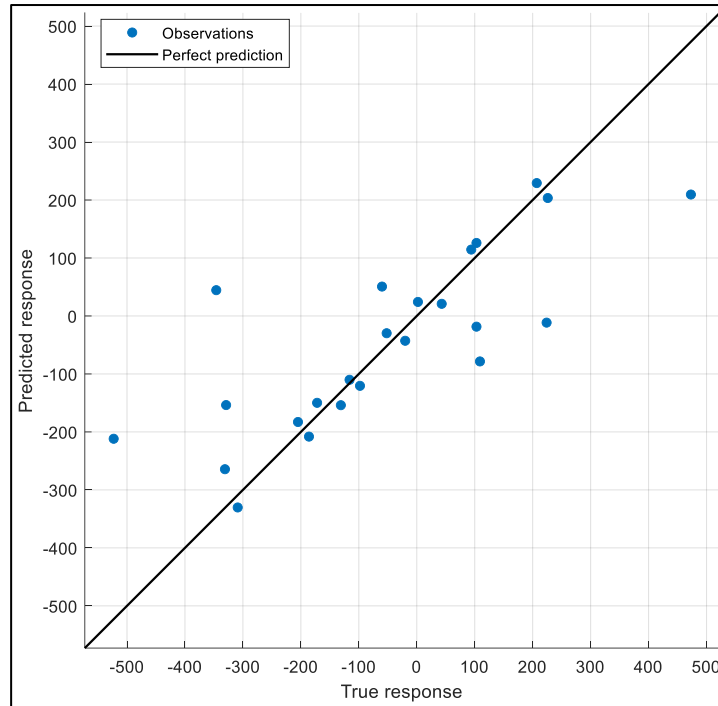


Figure 7 - SVM model for σ_{yy} (training phase by cubic kernel function).

Figures 6 and 7 indicate, respectively, the linear correlation concerning the observed and the estimated residual stresses σ_{xx} and σ_{yy} in the training stage. We accomplish that the training is suitably completed through the SV regression.

4.5 GPR model

We trained several GPR models under Regression Learner of Matlab, such as rational quadratic, squared exponential, Matern 5/2 and Exponential. The exponential model was selected because it gives better results than the others do.

Figures 8 and 9 show, respectively, the linear correlation between true and predictive responses of residual stresses σ_{xx} and σ_{yy} in the training stage. We accomplish that the training is perfectly completed through GPR for σ_{xx} , but it has difficulties in learning for σ_{yy} .

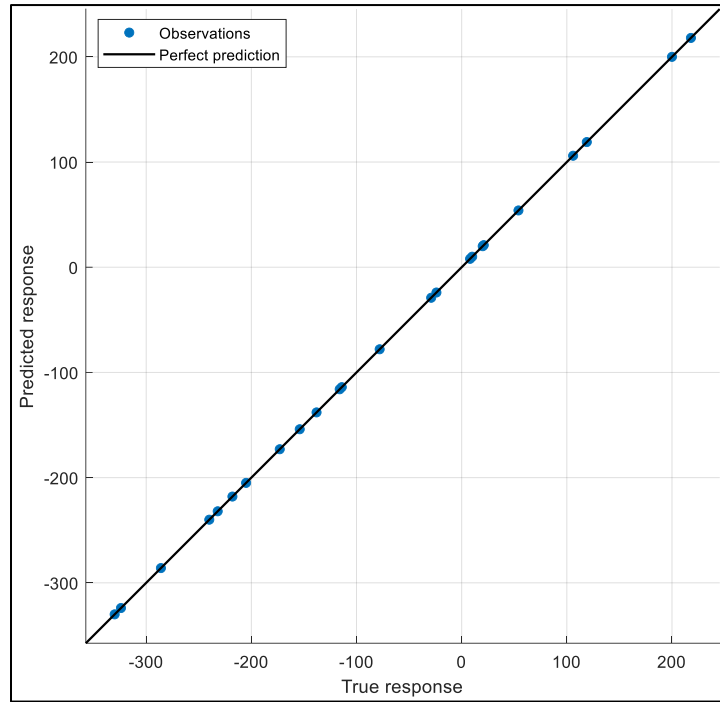


Figure 8 - GPR model for σ_{xx} (training phase by exponential kernel function).

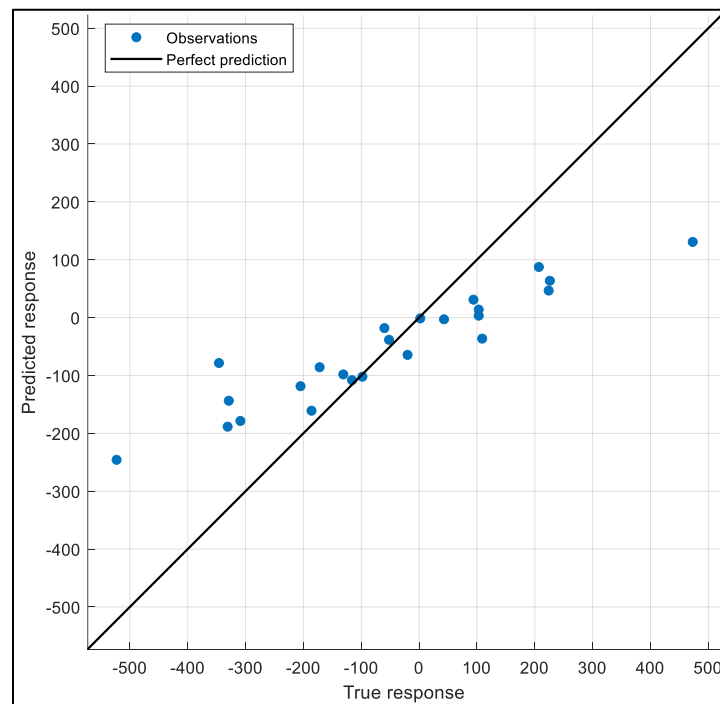


Figure 9 - GPR model for σ_{yy} (training phase by exponential kernel function).

5. Performance indicators of the predictive models

The performances of the developed models were evaluated by using the succeeding indicators: R^2 , MSE and MAPE (Makhfi *et al.*, 2018; Mimoun *et al.*, 2022; Djellouli *et al.*, 2023). We used these metrics to correlate the predictions with observed data.

- The R^2 statistic can be expressed by the following equation:

$$R^2 = 1 - \frac{SSR}{SST} = 1 - \frac{\sum_{k=1}^N (c(k) - s(k))^2}{\sum_{k=1}^N (c(k) - \bar{c})^2} \tag{17}$$

With c denotes experimental data of residual stresses, s represents the predictive values, \bar{c} is the mean of the observed data, and N is the entire number of tests or samples.

- The MSE is calculated by:

$$MSE = \frac{1}{N} \sum_{k=1}^N (c(k) - s(k))^2 \tag{18}$$

- The MAPE) is done by Equation 19:

$$MAPE(\%) = 100 \times \frac{1}{N} \sum_{k=1}^N \left| \frac{c(k) - s(k)}{c(k)} \right| \tag{19}$$

5.1 Confrontation of ANN, ANFIS, SVM and GPR models for the training and testing phases

Below are the simulation results for both training and testing phases. Tables 5 and 6 summarize the predictive capabilities of ANN, ANFIS, SVM and GPR models for σ_{xx} and σ_{yy} residual stresses.

Table 5 – Simulation results for the training.

Exp.	σ_{xx} (MPa)				Exp.	σ_{yy} (MPa)			
	ANN	ANFIS	SVM	GPR		ANN	ANFIS	SVM	GPR
106	81.77	106.00	123.04	105.99	94	75.93	94.00	114.52	30.99
54	44.95	54.00	36.94	53.98	-98	-81.17	-98.00	-120.49	-102.14
-205	-161.92	-205.00	-187.68	-204.98	-205	-138.19	-205.00	-182.86	-118.60
-24	-90.83	-24.00	-80.77	-24.02	-116	-130.96	-116.00	-110.07	-108.15
-114	-143.09	-114.00	-99.48	-114.01	-20	-120.59	-20.00	-42.77	-64.43
-29	-59.86	-29.00	-46.05	-29.02	207	222.35	207.00	229.20	87.42
-78	20.62	-77.99	18.43	-77.98	-60	-3.57	-59.99	50.70	-18.20
21	27.28	20.99	3.59	20.99	103	-62.69	103.00	-18.45	3.39
20	8.20	20.00	2.68	19.99	43	102.52	43.00	20.97	-3.01
119	74.59	119.00	101.80	118.97	226	242.42	226.00	203.46	63.66
8	57.44	8.00	25.09	8.00	-172	-100.25	-172.00	-149.80	-85.78
218	129.49	218.00	91.36	217.97	224	52.86	224.00	-11.50	46.69
200	198.26	200.00	217.35	199.98	-52	17.07	-52.00	-29.76	-38.37
10	24.80	10.00	27.07	10.01	2	107.89	2.00	24.22	-1.42
-138	-163.98	-138.00	-120.62	-137.99	-329	-286.30	-329.00	-153.66	-143.66
-154	-199.09	-154.00	-177.41	-154.01	-186	-299.58	-186.00	-208.08	-160.94

-232	-221.28	-232.00	-228.82	-231.99	-131	-162.25	-131.00	-153.88	-98.25
-286	-264.24	-286.00	-268.76	-285.98	103	68.33	103.00	125.95	13.84
-330	-245.31	-330.00	-192.51	-329.97	-523	-306.44	-523.00	-211.79	-245.77
-218	-226.19	-218.00	-234.93	-217.99	-309	-364.30	-309.00	-330.29	-178.63
-173	-198.98	-173.00	-190.13	-173.01	109	-49.74	109.00	-78.40	-36.38
-240	-250.14	-240.00	-222.74	-239.98	-331	-292.85	-331.00	-264.30	-188.50
-324	-222.55	-324.00	-171.02	-323.95	-346	-24.97	-346.00	44.50	-78.50
-116	-132.97	-116.00	-131.74	-116.01	473	236.69	473.00	209.45	130.74

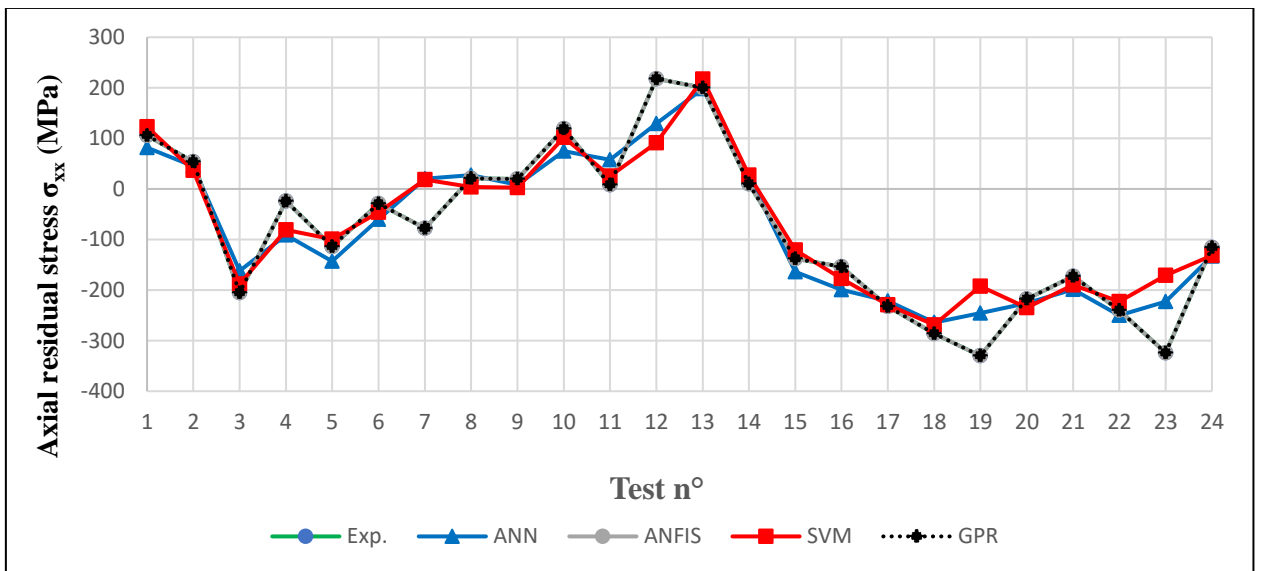


Figure 10 - Comparison among the experimental and predictive σ_{xx} (Training).

We notice through Table 5 and Figure 10 that the ANFIS and GPR models offer better learning capabilities; they correlate perfectly with the experimental data relating to σ_{xx} .

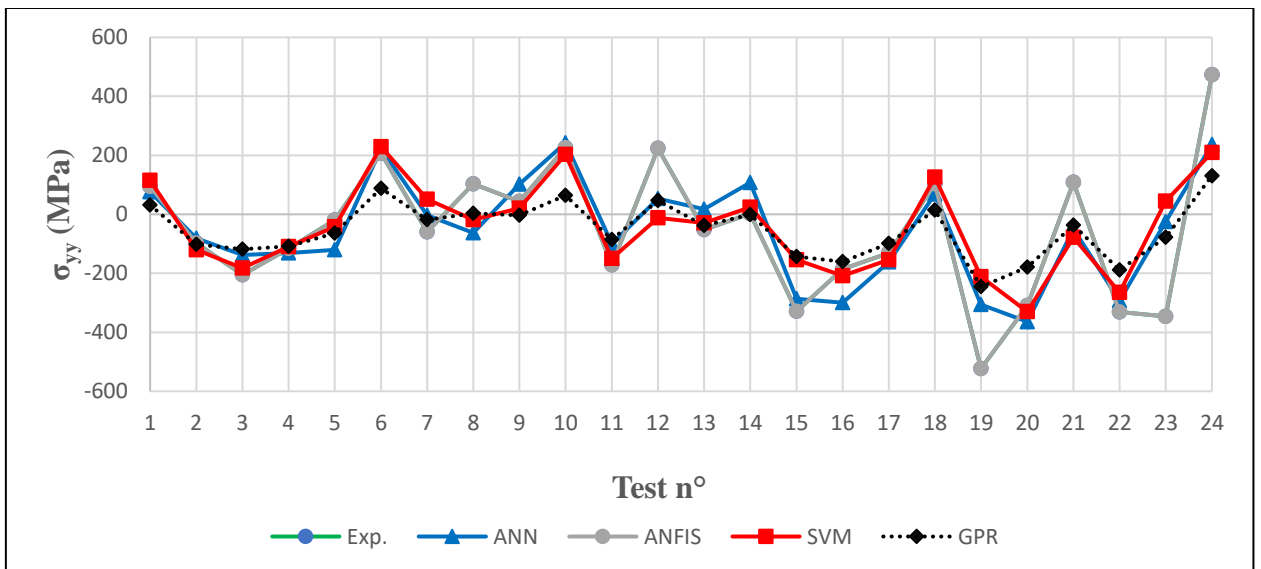


Figure 11 - Comparison among the experimental and predictive σ_{yy} (Training).

Figure 11 illustrates that during the training phase for σ_{yy} , ANFIS showed consistent ability to approximate experimental values more accurately.

Table 6 – Simulation results for the testing.

Exp.	σ_{xx} (MPa)				Exp.	σ_{yy} (MPa)			
	ANN	ANFIS	SVM	GPR		ANN	ANFIS	SVM	GPR
-17	-57.45	0.00	-71.36	-135.54	-99	-138.18	0.00	-124.59	-114.48
-68	-154.16	-114.96	-88.12	-105.42	-244	-272.68	-20.00	-68.88	-58.98
-127	-140.11	-98.00	-88.62	-165.69	48	-14.43	-58.43	69.43	-22.72
96	33.94	13.01	6.90	17.65	131	85.95	111.17	7.69	-3.73
0	57.97	9.23	20.28	41.20	23	76.80	130.15	1.34	2.20
-83	-75.57	-128.63	-110.09	-91.26	113	-32.56	-154.82	-108.98	-76.29
-188	-238.15	-185.03	-190.00	-196.75	-28	-238.82	-12.07	-157.06	-124.74
-379	-246.90	-261.23	-213.24	-175.59	108	-75.09	62.30	-73.91	-57.73
-479	-199.79	-260.09	-173.54	-149.89	-523	-213.95	-154.18	-159.14	-128.10
-280	-247.12	-412.02	-184.25	-204.00	-297	-179.86	-211.06	-77.48	-86.27

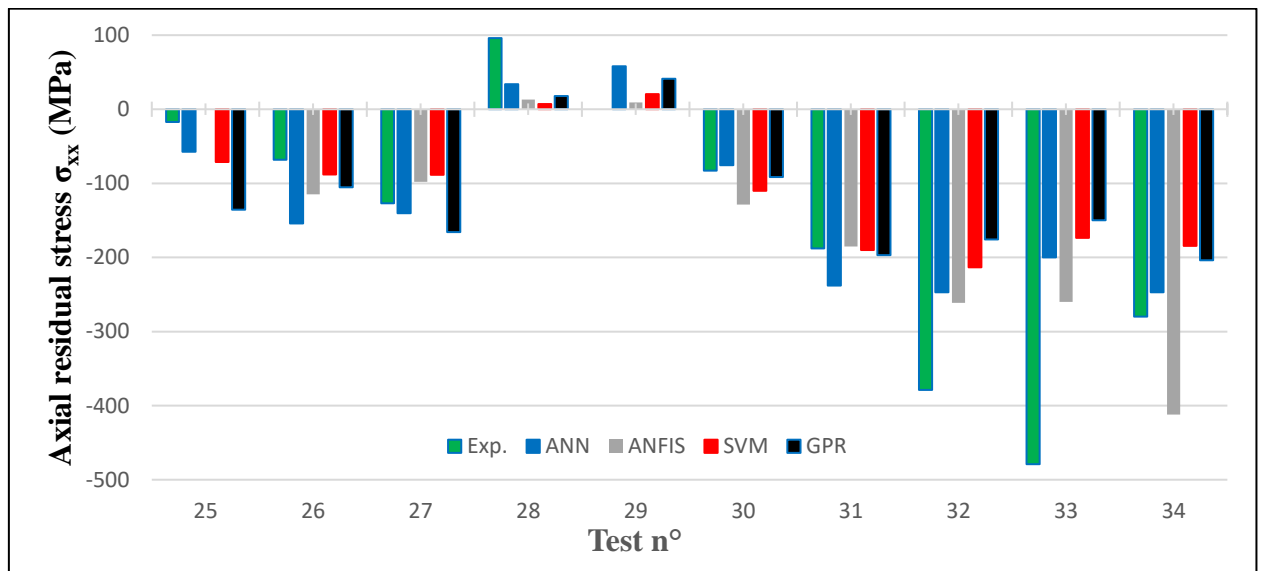


Figure 12 - Comparison among the experimental and predictive σ_{xx} (Testing).

We can see in Figure 12 that the predictions are consistent in terms of sign; nevertheless, there are notable discrepancies for the large residual stresses relating to tests 32 and 33. In addition, the ANN and ANFIS models have relatively the best performance.

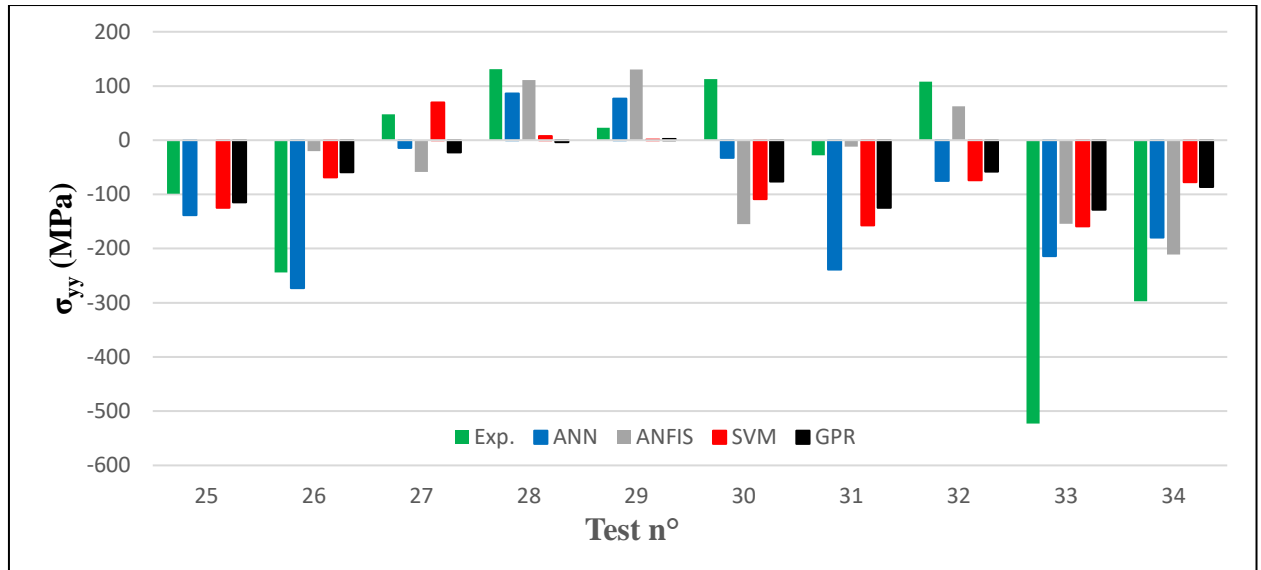


Figure 13 - Comparison among the experimental and predictive σ_{yy} (Testing).

Figure 13 shows that during the testing phase relating to σ_{yy} , the performances of all models declined with larger deviations from the experimental values. ANN and ANFIS continued to demonstrate stronger overall performance. This drop in accuracy highlights the challenges associated with generalizing the models beyond the training dataset.

5.2. Performances evaluation for the developed models of residual stresses

The following tables compare the performance of various predictive models used to estimate residual stresses. Notice that the performance evaluation for the training and testing phases provides valuable insights into how well each model approximates the experimental values.

Table 7 – Performance evaluation - training stage of σ_{xx} .

	ANN	ANFIS	SVM	GPR
MSE	2210.80138	7.44583E-06	3179.71383	0.00040267
MAPE	54.4394521	0.002970731	98.9220677	0.02341871
R²	0.90673686	1	0.86586307	1

Table 8 – Performance evaluation - training stage of σ_{yy} .

	ANN	ANFIS	SVM	GPR
MSE	14705.8041	4.82167E-06	19938.0076	19791.148
MAPE	205.340653	0.003603968	204.909942	345.372594
R²	0.70625302	1	0.60174027	0.60467378

Table 9 – Performance evaluation - testing phase of σ_{xx} .

	ANN	ANFIS	SVM	GPR
MSE	11550.4329	9161.8609	14387.223	18039.6662
MAPE	65.597014	138.2147457	186.569603	107.631899
R²	0.60363704	0.68560292	0.50629017	0.38095346

Table 10 – Performance evaluation - testing phase of σ_{yy} .

	ANN	ANFIS	SVM	GPR
MSE	21956.926	30065.984	32705.9036	33106.9074
MAPE	158.274464	133.0234281	457.12488	635.914672
R ²	0.47383809	0.27951774	0.21625638	0.20664697

Table 11 – Performance comparison for (σ_{xx}).

	ANN	ANFIS	SVM	GPR
MSE	4957.75181	2694.664977	6476.04004	5305.78445
MAPE	57.7210879	40.65349278	124.700755	31.6729718
R ²	0.81230581	0.897983403	0.75482534	0.79912973

Table 12 – Performance comparison for (σ_{yy}).

	ANN	ANFIS	SVM	GPR
MSE	16838.487	8842.93649	23693.2711	23707.5478
MAPE	191.497657	39.12708165	279.090806	430.826146
R ²	0.64714587	0.81469436	0.5035024	0.50320322

6. Conclusions

This study aims to develop effective models for predicting both axial and circumferential residual stresses during the hard turning of AISI 52100 steel with a CBN cutting tool. A comprehensive analysis was performed, comparing the performances of ANN, ANFIS, SVM and GPR models on a dataset derived from experimental machining. The models use for inputs various factors such as rheological coefficients (A, B and n) of work material and cutting parameters (cutting speed V_c , feed f and depth-of-cut a_p).

- For the training phase, ANFIS demonstrated exceptional accuracy ($R^2 = 1$) with minimal MSE and MAPE for both residual stresses.
- For the testing phase, ANFIS continued to yield best predictions for σ_{xx} , with R^2 value of 68.56%. ANN also exhibited good performances, with R^2 value of 60.36% for σ_{xx} and 47.38% for σ_{yy} . It should be noted that the performance of the ANFIS model decreased when predicting the residual stress σ_{yy} ($R^2 = 27.95\%$).
- Throughout this study, we validated our models against experimental values, demonstrating their potential applicability in estimating residual stresses during hard turning processes. The ANN and ANFIS models emerged as the most reliable approaches, providing high predictive accuracy and consistency. In conclusion, learning techniques particularly ANFIS exhibit strong promise for accurately predicting residual stresses in hard turning operations, suggesting valuable implications for optimizing machining processes.

References

- Ajay, C., Vikas S. (2020). Surface Integrity of AISI 52100 Steel during Hard Turning in Different Near-Dry Environments. *Advances in Materials Science and Engineering*, 4256308. <https://doi.org/10.1155/2020/4256308>
- Cristianini, N., Shawe-Taylor J. (2000). An Introduction to Support Vector Machines and Other Kernel-Based Learning Methods. *Cambridge University Press*. <https://doi.org/10.1017/CBO9780511801389>
- Cortes, C., Vapnik, V. (1995). Support-vector networks. *Mach Learn*, 20, 273–297. <https://doi.org/10.1007/BF00994018>

- Deng Z., Guo Z., Zhang X. (2017). Interval model updating using perturbation method and radial basis function neural networks. *Mechanical Systems and Signal Processing*, 84, 699-716. <https://doi.org/10.1016/j.ymsp.2016.09.001>
- Djellouli, K., Haddouche, K., Belarbi, M., & Aich, Z. (2023). Prediction of the cutting tool wear during dry hard turning of AISI D2 steel by using models based on Learning process and GA polyfit. *The Journal of Engineering and Exact Sciences*, 9(12). 18297. <https://doi.org/10.18540/jcecv19iss12pp18297>
- Gholami, R., Fakhari, N. (2017). Support Vector Machine: Principles, Parameters, and Applications. In: *Handbook of Neural Computation Elsevier*, 515–535. <https://doi.org/10.1016/B978-0-12-811318-9.00027-2>
- Gunn S. R. (1998). Support Vector Machines for classification and regression. *Technical Report, University of Southampton*. https://meandmyheart.wordpress.com/wp-content/uploads/2009/02/svm_gunn1.pdf
- Habak, M. (2006). *Etude de l'influence de la microstructure et des paramètres de coupe sur le comportement en tournage dur de l'acier à roulement 100Cr6*. Thèse de Doctorat, École Nationale Supérieure d'Arts et Métiers, France.
- Hagan, M. T., Demuth, H. B., Beale, M. H., De Jesús, O. (2014). *Neural Network Design*. 2nd Edition eBook.
- Hsu C-W., Chang C-C., Lin C-J. (2016). A practical guide to support vector classification. Technical report, National Taiwan University. <http://www.csie.ntu.edu.tw/~cjlin>.
- Huang, X., Yansong, Z., Daode, Z., Jing, X., Wen-qiong, Z., Shengnan, L., Zihang, Y. (2023). Effects of multi-pass turning on surface properties of AISI 52100 bearing steel. *The International Journal of Advanced Manufacturing Technology*, 127(3-4), 1823-1833. <https://doi.org/10.1007/s00170-023-11677-7>
- Hüseyin Alp, Ç., Adem Ç., Necati U., Kubilay A. (2024). Performance of conventional and wiper CBN inserts under various cooling conditions in hard turning of AISI 52100 steel. *Materials Testing*, 66(2), 288-298. <https://doi.org/10.1515/mt-2023-0263>
- Isabona, J., Imoize, A. L., Ojo, S., Do, D-T., Lee, C-C.. (2023). Machine Learning-Based GPR with LBFSGS Kernel Parameters Selection for Optimal Throughput Mining in 5G Wireless Networks. *Sustainability*, 15, 1678. <https://doi.org/10.3390/su15021678>
- Jang, J.-s. R. (1993). ANFIS: Adaptive-network-based fuzzy inference system. *IEEE Transactions on Systems, Man, & Cybernetics*, 23(3), 665–685. <https://doi.org/10.1109/21.256541>
- Kara, F., Adem Çiçek A., and Halil Demir H. (2023). Effect of Deep Cryogenic Treatment on Microstructure, Mechanical Properties, and Residual Stress of AISI 52100 Bearing Steel. *Engineered Science*. 26. <https://doi.org/10.30919/es960>
- Kokkiralala, S., Holmberg, J., Klement, U. (2022). Effect of cutting parameters on the generated surface integrity of hard-turned martensitic AISI 52100 bearing steel. *Procedia CIRP*, 115: 154-159. <http://dx.doi.org/10.1016/j.procir.2022.10.066>.
- Makhfi, S. (2018). *Modélisation et simulation du comportement thermomécanique de l'usinage à grande vitesse*. Thèse de Doctorat, Université de Tlemcen, Algérie.
- Makhfi, S., Haddouche, K., Bourdim, A., Habak, M. (2018). Modeling of machining force in hard turning process. *Mechanika*, 24, 3, 367-375. <http://dx.doi.org/10.5755/j01.mech.24.3.19146>
- Mimoun, C. H., Haddouche, K., Makhfi, S. (2022). A Comparative Study of Multiple Regression, ANN and Response Surface Method for Machining Force. Proc. of the Interdisciplinary Conference on Mechanics, Computers and Electrics (ICMECE 2022) 6-7 October 2022, Barcelona, Spain. <http://www.icmece.org/2022/proceedings.pdf>.
- Outeiro, J. (2018). Residual stresses in machining operations. *CIRP Encyclopedia of Production Engineering; Laperrière, L, Reinhart, G, Eds*. Springer, Berlin, Heidelberg, 1-13. https://doi.org/10.1007/978-3-642-35950-7_16811-1

- Paschoalinoto N. W. , Bordinassi E. C., Bortolussi R., Leonardi F., Delijaicov S. (2021). The effect of process parameters and cutting tool shape on residual stress of SAE 52100 hard turned steel by high speed machining. *Proceedings of the Institution of Mechanical Engineers, Part B: Journal of Engineering Manufacture*, 235(1-2), 290-300.
<http://dx.doi.org/10.1177/0954405420929788>
- Pawar S., Salve A., Chinchankar S., Kulkarni A., Lamdhade G., (2017). Residual Stresses during Hard Turning of AISI 52100 Steel: Numerical Modelling with Experimental Validation. *Materials Today: Proceedings*, Part A 4(2), 2350-2359.
<https://doi.org/10.1016/j.matpr.2017.02.084>
- Salcedo-Sanz, S., Rojo-Álvarez, J. L., Martínez-Ramón, M., Camps-Valls, G. (2014). Support vector machines in engineering: an overview. *WIREs Data Min & Knowledge Discovery*, 4, 234–267. <https://doi.org/10.1002/widm.1125>
- Schulz, E., Speekenbrink, M., Krause, A. A. (2018). Tutorial on Gaussian process regression: Modelling, exploring, and exploiting functions. *Journal of Mathematical Psychology*, 1-16.
<https://doi.org/10.1101/095190>
- Sivaraman, V., Prakash, S. (2017). Recent developments in turning hardened steels – A review. *Frontiers in Automobile and Mechanical Engineering. IOP Conf. Series: Materials Science and Engineering*, 197. <https://doi.org/10.1088/1757-899X/197/1/012009>
- Soori, M. Arezoo, B. (2022). A Review in Machining-Induced Residual Stress *Journal of New Technology and Materials*, 12(01), 64-83. <https://hal.science/hal-03679993v1>
- Sutanto, H., Madl, J., (2018). Residual stress development in hard machining-a review. *IOP Conference Series: Materials Science and Engineering. IOP Publishing*.
<https://doi.org/10.1088/1757-899X/420/1/012031>
- Vapnik V. N., (1998). *Statistical Learning Theory*. Wiley-Interscience.
- Tabatabaeian, A., Ghasemi, A. R., Shokrieh, M. M., Marzbanrad, B., Baraheni, M., & Fotouhi, M. (2022). Residual stress in engineering materials: A review. *Advanced Engineering Materials*, 24(3), 2100786. <https://doi.org/10.1002/adem.202100786>